Polyhedron 151 (2018) 243–254

Contents lists available at ScienceDirect

Polyhedron

journal homepage: www.elsevier.com/locate/poly

Novel dichloro(bis{2-[1-(4-methylphenyl)-1H-1,2,3-triazol-4-yl-κN^3]pyridine-κN})metal(II) coordination compounds of seven transition metals (Mn, Fe, Co, Ni, Cu, Zn and Cd)

J. Conradie [a,*], M.M. Conradie [a], K.M. Tawfiq [b,c], M.J. Al-Jeboori [c], S.J. Coles [d], C. Wilson [e], J.H. Potgieter [b,f,*]

[a] Department of Chemistry, University of the Free State, P.O. Box 339, Bloemfontein 9300, South Africa
[b] Division of Chemistry and Environmental Science, Manchester Metropolitan University, Manchester M1 5GD, UK
[c] Department of Chemistry, College of Education for Pure Science (Ibn Al-Haitham), University of Baghdad, Baghdad, Iraq
[d] EPSRC National Crystallography Service, Chemistry, University of Southampton, Southampton SO17 1BJ, England, UK
[e] School of Chemistry, University of Glasgow, Joseph Black Building, University Avenue, Glasgow G12 8QQ, Scotland, UK
[f] School of Chemical and Metallurgical Engineering, University of the Witwatersrand, Private Bag X3, Wits 2050, South Africa

ARTICLE INFO

Article history:
Received 23 December 2017
Accepted 25 March 2018
Available online 3 April 2018

Keywords:
(1,2,3-Triazol-4-yl)pyridine
Coordination compound
DFT
Bonding-path
Donor–acceptor

ABSTRACT

The synthesis, characterization, DFT and, in two cases, the structure of seven novel dichloro(bis{2-[1-(4-methylphenyl)-1H-1,2,3-triazol-4-yl-κN^3]pyridine-κN})metal(II) coordination compounds ([M(L^2)$_2$Cl$_2$]), containing transition metals of groups 7–12, are described. Both experimentally measured magnetic moment and DFT calculations showed that d^5 Mn(II) (with μ_{eff} = 5.62 B.M., *S* = 5/2), d^6 Fe(II) (with μ_{eff} = 5.26 B.M., *S* = 2), d^7 Co(II) (with μ_{eff} = 3.98 B.M., *S* = 3/2), d^8 Ni(II) (with μ_{eff} = 3.00 B.M., *S* = 1) and d^9 Cu(II) (with μ_{eff} = 1.70 B.M., *S* = ½) are all paramagnetic, while d^{10} Zn(II) and Cd(II) are diamagnetic with *S* = 0. DFT calculations on the possible isomers of these coordination compounds, showed that the *cis–cis–trans* and the *trans–trans–trans* isomers, with the pyridyl groups *trans* to each other, are the lowest in energy. The *trans–trans–trans* isomers were experimentally characterized by X-ray crystallography for [Ni(L^2)$_2$Cl$_2$] and [Zn(L^2)$_2$Cl$_2$]·L^2 in this study. In the solid state the coordination compounds are connected by intermolecular hydrogen bonds, mainly involving the chloride atoms, to form 3D supramolecular structures. Computational chemistry calculations, using Natural Bonding Orbital calculations, identified these inter-molecular hydrogen bonds, C—H···Cl, by a donor–acceptor interaction from a filled lone pair NBO on Cl to an empty antibonding NBO on (C—H). The inter-molecular hydrogen bonds were also identified by QTAIM determined bonding paths between Cl and the respective hydrogen. The theoretically calculated computational chemistry results thus give an understanding on a molecular level why in the solid state where inter-molecular forces and packing play a role, the *trans–trans–trans* isomers are mostly obtained.

1. Introduction

The 1,3-dipolar cycloaddition "click" reaction between an azide and an alkyne to give a 1,2,3-triazole was reported by Huisgen in 1961 [1]. In 2002 the Copper(I)-catalyzed Azide-Alkyne Cycloaddition (CuAAC) to prepare a 1,2,3-triazole was reported [2,3]. The existence of relatively basic nitrogen atoms in the 1,2,3-triazole rings, and the possibility of introducing additional donor groups in the substituents (Fig. 1), made the CuAAC "click" reaction an attractive method to prepare differently substituted 1,2,3-triazoles. These compounds have been used as ligands to coordinate to various metal ions that display a range of applications such as in electrochemical and photochemical studies, in supramolecular chemistry, magnetism, metal-ion sensing and catalysis [4]. The reasons for the success of the "click" reaction, is that it is easy to carry out and is widely applicable. It is not affected by a variety of functional groups, and can be carried out with a variety of Cu(I) catalysts and solvents, including aqueous conditions. The Cu(I) catalysts overcome the high activation energy barrier of the non-catalyzed Huisgen reaction by changing the mechanism of the reaction. A large variety of copper catalysts can be used for the CuAAC reaction, on condition that the maximum concentration of Cu(I) species is generated during the reaction. The pre-catalyst

* Corresponding authors at: Department of Chemistry, University of the Free State, P.O. Box 339, Bloemfontein 9300, South Africa (J. Conradie); Division of Chemistry and Environmental Science, Manchester Metropolitan University, Manchester M1 5GD, UK (J.H. Potgieter).

E-mail address: conradj@ufs.ac.za (J. Conradie).

https://doi.org/10.1016/j.poly.2018.03.026
0277-5387/

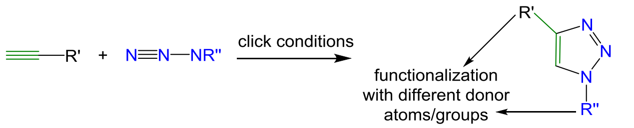

Fig. 1. The Cu(I) catalyzed "click" reaction between an azide and alkyne to produce a 1,2,3-triazole that can be functionalized with different donor atoms or groups.

can be a Cu(II) salt (usually $CuSO_4$) together with a reducing agent (often sodium ascorbate) or a Cu(I) compound in the presence of a base or amine ligand and a reducing agent to prevent oxidation to Cu(II). Some strong oxidising cupric salts or complexes such as $Cu(OAc)_2$ also work. The solvent is very flexible from organic to aqueous, with the most commonly used combination water + an alcohol (*t*-BuOH, MeOH or EtOH). The key role of the solvent or solvent mixture is to solubilize the substrates and Cu(I) catalyst in order to ensure rapid reactions. Such aqueous conditions are very useful for biochemical conjugations, as well as for organic syntheses.

We recently reported on the synthesis of a series of differently substituted 1,2,3-triazole chromophores, the substituted 2-(1-phenyl-1H-1,2,3-triazol-4-yl)pyridine ligands [5], see Fig. 2 middle, with substituents R = H (L^1), CH_3 (L^2), OCH_3 (L^3), COOH, F, Cl, CN, CF_3, $O(CH_2)_3CH_3$ and $N(CH_3)_2$. These versatile ligands were found to coordinate to various first row transition metals, such as manganese, cobalt and nickel [6]. Here we extend the series to include more first row transition metal(II) coordination compounds, iron, copper and zinc, as well as a second row transition metal(II) coordination compound, cadmium, containing the 2-(1-(4-methyl-phenyl)-1H-1,2,3-triazol-1-yl)pyridine chromophore (Fig. 2 right with R = CH_3). This series of seven novel coordination compounds is the first series of pyridyl-triazole based transition metal coordination compounds where seven different transition metals are coordinated to the same 1,2,3-triazole chromophore, namely 2-(1-(4-methyl-phenyl)-1H-1,2,3-triazol-1-yl)pyridine.

2. Methods and materials

2.1. Synthesis of 2-(1-(4-methyl-phenyl)-1H-1,2,3-triazol-1-yl) pyridine (L^2)

The ligand, 2-(1-(4-methyl-phenyl)-1H-1,2,3-triazol-1-yl)pyridine (L^2), was synthesized and characterized as described previously [5,7]. A mixture of 1-azido-4-methylbenzene (0.75 g; 5.63 mmol) and 2-ethynylpyridine (0.69 g; 6.75 mmol, 1.2 eq) was dissolved in a 1:1 mixture of water/tert–butyl alcohol (100 ml). After stirring for 20 min, a solution of $CuSO_4.5H_2O$ (0.41 g; 1.64 mmol) in water (10 ml) was added dropwise followed by a freshly prepared solution of Na-ascorbate (0.37 g; 1.85 mmol) in water (5 ml). The mixture was allowed to stir for 24 h at RT, and then an aqueous ammonia solution (15%; 50 ml) was added. The mixture was stirred for a further 20 min, and then extracted with dichloromethane (2 × 100 ml). The organic phase was washed twice with water (2 × 100ml) and filtered through Celite to remove trapped Cu(I)-salts ($[Cu(NH_3)_6]^+$). The combined organic layer was washed with brine (2 × 100 ml), and then dried over $MgSO_4$. The organic solvent was removed under vacuum to give the crude product as a bright yellow solid with yield of (0.98 g; 74%). Recrystallisation from a mixture of CH_2Cl_2:CH_3OH (1:1) gave the product as colourless crystals (0.93 g; 70%), mp. 128–129 °C. ATR/IR: $\overline{\nu}(cm^{-1})$: 3128, 3099, 2947, 2919, 1597, 1592, 1566, 1543, 1471, 1271, 1238, 1212, 1176, 1148, 1036, 998, 813 and 784, 745. NMR data (ppm), δ_H (400 MHZ, CD_2Cl_2-d_2): 8.60–8.58 (1H, ddd, $^1J_{HH}$ = 0.92 Hz, $^2J_{HH}$ = 1.83 Hz, $^3J_{HH}$ = 5.04 Hz, H_{14}), 8.57 (1H, s, H_8), 8.21–8.18 (1H, td, $^1J_{HH}$ = 0.92 Hz, $^2J_{HH}$ = 1.37 Hz, $^3J_{HH}$ = 7.79 Hz, H_{11}), 7.82–7.77 (1H, dt, $^1J_{HH}$ = 1.83 Hz, $^2J_{HH}$ = 7.79 Hz, H_{12}), 7.70–7.67 (2H, d, J_{HH} = 8.70 Hz, Ar-$H_{2,6}$), 7.35–7.33 (2H, d, J_{HH} = 8.24 Hz, Ar-$H_{3,5}$), 7.26–7.23 (1H, ddd, $^1J_{HH}$ = 1.37 Hz, $^2J_{HH}$ = 4.58 Hz, ^3J = 7.33, H_{13}), 2.41 (3H, s, CH_3, H_7); δ_c (100.63 MHZ, CD_2Cl_2-d_2): 21.14 (C_7), 120.34 (C_{11}), 120.37 (C_8), 120.56 (C_3,C_5), 123.26 (C_{13}), 130.56 (C_2,C_6), 135.05 (C_4), 137.13 (C_{12}), 139.40 (C_1), 149.14 (C_9), 149.89 (C_{14}), 150.48 (C_{10}). These assignments were confirmed using DEPT ^{13}C (135°), ^1H–^1H COSY and ^1H–^{13}C HMQC two-dimensional correlations. HRMS (P + NSI): $[M+H]^+$ (100%): *m/z* = 237.1135 calculated for ($C_{14}H_{13}N_4$); found 237.1133. The fragment of the molecular ion plus H^+ $[(M-N_2)+H]^+$ (15%): calculated for ($C_{14}H_{13}N_2$); found *m/z* = 209.1133.

2.2. Synthesis of the 2-(1-(4-methylphenyl)-1H-1,2,3-triazol-1-yl) pyridine-metal coordination compounds $[M(L^2)_2Cl_2]$

*2.2.1. Dichloro(bis{2-[1-(4-methylphenyl)-1H-1,2,3-triazol-4-yl-κN^3] pyridine-κN})manganese(II) (**1**)*

$[Mn(L^2)_2Cl_2]$ was prepared by stirring a solution of anhydrous $MnCl_2$ (0.041 g, 0.32 mmol) in CH_3OH (10 ml). A solution of the

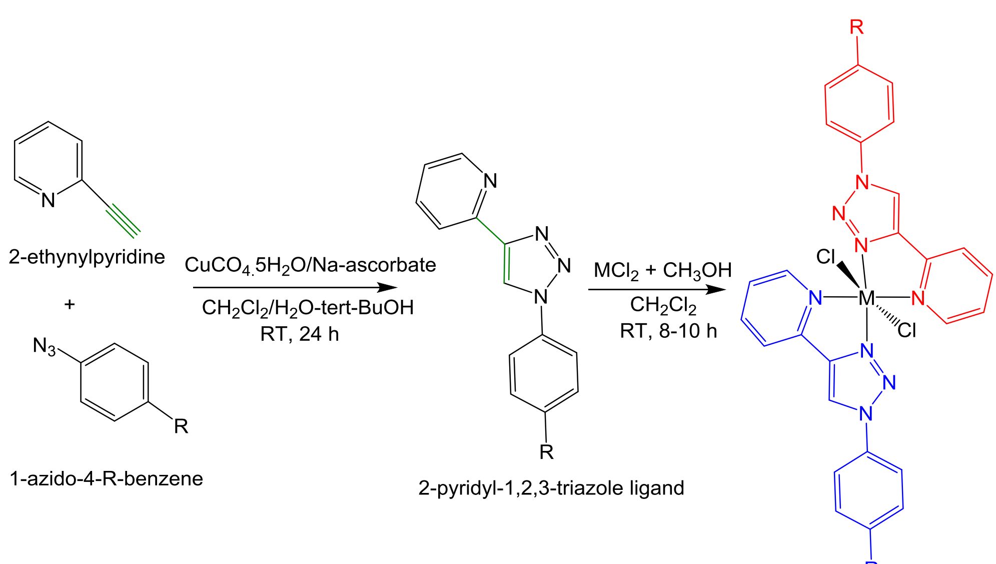

Fig. 2. Synthesis of 2-pyridyl-(1,2,3)-triazole ligands from an azide and alkyne by the Cu(I) catalyzed "click" reaction (reaction left). Synthesis of the various dichloro(bis{2-[1-(4-R-phenyl)-1H-1,2,3-triazol-4-yl–κN^3]pyridine-κN})metal(II) coordination compounds, M = Mn (1), Fe (2), Co (3), Ni (4), Cu (5), Zn (6) and Cd (7) (reaction right), with the structure of 1,2,3-triazole chromophores, 2-(1-(4-R-phenyl)-1H-1,2,3-triazol-1-yl)pyridine shown in the middle. R = H for the ligand L^1, and R = CH_3 for the ligand L^2.

ligand L^2 (0.15 g, 0.65 mmol, 2 eq) in CH_2Cl_2 (10 ml), was added dropwise to it. A resulting pale yellow precipitate was obtained after stirring for 8–10 h at RT. The solvent was then reduced in volume by a half under vacuum distillation before it was filtered and washed twice with cold methanol and then diethyl ether. A pale yellow solid was obtained and isolated to yield a precipitate that give (0.195 g, 0.32 mmol, yielded 80%), mp. 324–326 °C. ATR/IR: $\overline{\nu}(cm^{-1})$: 3068, 3055, 3022, 1606, 1595, 1575, 1521, 1473, 1446, 1253, 1253, 1062, 1044, 1011, 1000, 979, 861, 812, 784, 719. UV–Vis (DMSO) λ_{max}: $[Mn(L^2)_2Cl_2]$ showed absorption bands at 257 nm, ε_{max} = 88 450 $dm^3\ mol^{-1}\ cm^{-1}$, 287 nm, ε_{max} = 40 200 $dm^3\ mol^{-1}\ cm^{-1}$, 682 nm, ε_{max} = 13 $dm^3\ mol^{-1}\ cm^{-1}$. $[Mn(L^2)_2Cl_2]$ showed a value of μ_{eff} = 5.62 B.M. HRMS TOF (ESI+) (water:acetonitrile = 1:3) with the highest molecular weight ion peak matching, was observed at m/z = 562.1202 (80%) and is related to $[[Mn(L^2)_2Cl_2]-Cl]^+$. The calculated value for $[C_{28}H_{24}ClMnN_8]^+$ is 562.1193. Λ_M (DMSO) = 50 $\Omega^{-1}cm^2mol^{-1}$. Elemental *Anal.* Calc. for $C_{28}H_{24}N_8Cl_2Mn$: C, 56.2; H, 4.0; N, 18.7. Found: C, 56.0; H, 4.1; N, 18.4%.

2.2.2. Dichloro(bis{2-[1-(4-methylphenyl)-1H-1,2,3-triazol-4-yl-κN³] pyridine-κN})iron(II) (**2**)

For the preparation of $[Fe(L^2)_2Cl_2]$, the method used was analogous to that for $[Mn(L^2)_2Cl_2]$. An amount of 0.041 g, 0.32 mmol of anhydrous $FeCl_2$ and 0.15 g, 0.63 mmol of L^2 were used, and an identical work-up procedure gave the required compound as a bright yellow solid. The isolated precipitate gave (0.20 g, 0.33 mmol, yield 83%), mp. 310–312 °C. ATR/IR: $\overline{\nu}(cm^{-1})$; 3063, 3047, 3025, 1605, 1595, 1571, 1522, 1473, 1448, 1267, 1258, 1063, 1054, 1015, 1004, 886, 815, 786, 553. UV–Vis (DMSO) λ_{max}: $[Fe(L^2)_2Cl_2]$ showed absorption bands at 259 nm, ε_{max} = 65 500 $dm^3\ mol^{-1}\ cm^{-1}$, 287 nm, ε_{max} = 52 000 $dm^3\ mol^{-1}\ cm^{-1}$, 326 nm, ε_{max} = 4783 $dm^3\ mol^{-1}\ cm^{-1}$, 908 nm, ε_{max} = 85 $dm^3\ mol^{-1}\ cm^{-1}$. $[Fe(L^2)_2Cl_2]$ showed a value of μ_{eff} = 5.26 B.M. HRMS TOF (ESI+) (water:acetonitrile = 1:3) with the highest molecular weight ion peak matching, was observed at m/z = 563.1135 (80%) and is attributed to $[[Fe(L^2)_2Cl_2]-Cl]^+$. The calculated value for $[(C_{28}H_{24}N_8MnCl)]^+$ is 563.1162. Λ_M (DMSO) = 43 $\Omega^{-1}\ cm^2\ mol^{-1}$. Elemental *Anal.* Calc. for $C_{28}H_{24}N_8Cl_2Fe$: C, 56.1; H, 4.0; N, 18.7. Found: C, 56.0; H, 4.1; N, 18.8%.

2.2.3. Dichloro(bis{2-[1-(4-methylphenyl)-1H-1,2,3-triazol-4-yl-κN³] pyridine-κN})cobalt(II) (**3**)

For the preparation of $[Co(L^2)_2Cl_2]$, the method used was analogous to that for $[Mn(L^2)_2Cl_2]$. An amount of 0.060 g, 0.21 mmol of $CoCl_2{\cdot}6H_2O$ and 0.11 g, 0.50 mmol of L^2 were used, and an identical work-up procedure gave the required compound as a bright pink solid. The isolated precipitate gave (0.11 g, 0.18 mmol, yield 73%), mp. 346–348 °C. ATR/IR: $\overline{\nu}(cm^{-1})$; 3045, 3024, 1609, 1595, 1575, 1522, 1475, 1450, 1262, 1245, 1065, 1056, 1018, 1005, 871, 814, 786, 755. UV–Vis (DMSO): The $[Co(L^2)_2Cl_2]$ showed absorption bands at 252 nm, ε_{max} = 45 200 $dm^3\ mol^{-1}\ cm^{-1}$, 257 nm, ε_{max} = 77 100 $dm^3\ mol^{-1}\ cm^{-1}$, 287 nm, ε_{max} = 26 967 $dm^3\ mol^{-1}\ cm^{-1}$, 615 nm, ε_{max} = 56 $dm^3\ mol^{-1}\ cm^{-1}$, 678 nm, ε_{max} = 89 $dm^3\ mol^{-1}\ cm^{-1}$. The $[Co(L^2)_2Cl_2]$ showed a value of μ_{eff} = 3.98 B.M. HRMS TOF (MALDI) with the highest molecular weight ion peak matching, was observed at m/z = 566.1 (100%) and is related to $[[Co(L^2)_2Cl_2]-Cl]^+$. The calculated value for $[(C_{28}H_{24}N_8FeCl)]^+$ is 566.1. Λ_M (DMSO) λ_{max} = 48 $\Omega^{-1}\ cm^2\ mol^{-1}$. Elemental *Anal.* Calc. for $C_{28}H_{24}N_8Cl_2Co$: C, 55.8; H, 4.0; N, 18.6. Found: C, 55.9; H, 3.9; N, 18.8%.

2.2.4. Dichloro(bis{2-[1-(4-methylphenyl)-1H-1,2,3-triazol-4-yl-κN³] pyridine-κN})nickel(II) (**4**)

For the preparation of $[Ni(L^2)_2Cl_2]$, the method used was as described for $[Mn(L^2)_2Cl_2]$. An amount of 0.050 g, 0.21 mmol of $NiCl_2{\cdot}6H_2O$ and 0.10 g, 0.42 mmol of L^2 were used, and an identical work-up procedure gave the required compound as a pale blue solid. The isolated precipitate gave (0.11 g, 0.18 mmol, yield 73%), mp. 340 °C (decomp.). ATR/IR: $\overline{\nu}(cm^{-1})$; 3038, 3021, 3010, 1612, 1596, 1577, 1521, 1476, 1451, 1264, 1247, 1067, 1058, 1007, 874, 813, 786, 756, 720. UV–Vis (DMSO) λ_{max}: $[Ni(L^2)_2Cl_2]$ showed absorption bands at 257 nm, ε_{max} = 102 150 $dm^3\ mol^{-1}\ cm^{-1}$, 285 nm, ε_{max} = 42 300 $dm^3\ mol^{-1}\ cm^{-1}$, 408 nm, ε_{max} = 18 $dm^3\ mol^{-1}\ cm^{-1}$, 668 nm, ε_{max} = 9 $dm^3\ mol^{-1}\ cm^{-1}$. $[Ni(L^2)_2Cl_2]$ showed a value of μ_{eff} = 3.00 B.M. HRMS TOF (ESI+) (water:acetonitrile = 1:3) with the highest molecular weight ion peak matching, was observed at m/z = 565.1167 (40%) and is related to $[[Ni(L^2)_2Cl_2]-Cl]^+$. The calculated value for $[(C_{28}H_{24}N_8NiCl)]^+$ is 565.1166. Λ_M (DMSO) = 45 $\Omega^{-1}\ cm^2\ mol^{-1}$. Elemental *Anal.* Calc. for $C_{28}H_{24}N_8Cl_2Ni$: C, 55.9; H, 4.0; N, 18.6. Found: C, 55.8; H, 4.0; N, 18.5%. A good single crystal for X-ray structural analysis was obtained by slow evaporation of a hot DMSO:CH_3CN = 1:9 solution of the $[Ni(L^2)_2Cl_2]$.

2.2.5. Dichloro(bis{2-[1-(4-methylphenyl)-1H-1,2,3-triazol-4-yl-κN³] pyridine-κN})copper(II) (**5**)

For the preparation of $[Cu(L^2)_2Cl_2]$, the method used was similar to that for $[Mn(L^2)_2Cl_2]$. An amount of 0.062 g, 0.46 mmol of anhydrous $CuCl_2$ and 0.21 g, 0.92 mmol of L^2 were used, and an identical work-up procedure gave the required compound as a pale green solid. The isolated precipitate gave (0.24 g, 0.39 mmol, yield 91%), mp. 274–276 °C. ATR/IR: $\overline{\nu}(cm^{-1})$; 3068, 3058, 3025, 1606, 1594, 1575, 1516, 1477, 1449, 1267, 1250, 1063, 1042, 1029, 862, 817, 779, 754, 716. UV–Vis (DMSO) λ_{max}: $[Cu(L^2)_2Cl_2]$ showed absorption bands at 257 nm, ε_{max} = 52 222 $dm^3\ mol^{-1}\ cm^{-1}$, 286 nm, ε_{max} = 35 556 $dm^3\ mol^{-1}\ cm^{-1}$, 908 nm, ε_{max} = 85 $dm^3\ mol^{-1}\ cm^{-1}$. $[Cu(L^2)_2Cl_2]$ showed a value of μ_{eff} = 1.70 B.M. HRMS (P+NSI); $(CH_3OH)/(NH_4OAC)$ with the highest molecular weight ion peak matching, was observed at m/z = 594.1547 (45%) and is attributed to $[(Cu(L^2)_2)^+ + (CH_3COO^-)]^+$. The calculated value for $[C_{28}H_{24}CuN_8]^+ + (CH_3COO^-)]^+$ is 594.1540. Λ_M (DMSO) = 31 $\Omega^{-1}\ cm^2\ mol^{-1}$. Elemental *Anal.* Calc. for $C_{28}H_{24}N_8Cl_2Cu$: C, 55.4; H, 4.0; N, 18.5. Found: C, 55.2; H, 4.1; N, 18.6%.

2.2.6. Dichloro(bis{2-[1-(4-methylphenyl)-1H-1,2,3-triazol-4-yl-κN³] pyridine-κN})zinc(II) (**6**)

For the preparation of $[Zn(L^2)_2Cl_2]$, the method used was as described for that of the $[Mn(L^2)_2Cl_2]$. An amount of anhydrous $ZnCl_2$ of 0.19 g, 1.40 mmol and 0.66 g, 2.8 mmol of L^2 were used, and an identical work-up procedure gave the required compound as a white solid. The isolated precipitate gave (0.18 g, 0.39 mmol, yield 78%), mp. 318–320 °C. ATR/IR: $\overline{\nu}(cm^{-1})$; 3064, 3041, 3021, 1607, 1570, 1517, 1475, 1448, 1270, 1239, 1073, 1055, 1075, 1006, 864, 812, 774, 754, 718. UV–Vis (DMSO) λ_{max}: $[Zn(L^2)_2Cl_2]$ showed absorption bands at 258 nm, ε_{max} = 47 931 $dm^3\ mol^{-1}cm^{-1}$, 288 nm, ε_{max} = 31 379 $dm^3\ mol^{-1}\ cm^{-1}$. NMR data (ppm), δ_H (400 MHZ, DMSO-d_6): 9.23 (1H, s, H_8), 8.66–8.65 (1H, d, J_{HH} = 4.12 Hz, H_{14}), 8.11–8.09 (1H, dd, $^1J_{HH}$ = 7.79 Hz, $^2J_{HH}$ = 0.92 Hz, H_{11}), 7.97–7.92 (1H, dt, $^1J_{HH}$ = 7.79 Hz, $^2J_{HH}$ = 1.83 Hz, H_{12}), 7.89–7.87 (2H, d, J_{HH} = 8.24 Hz, Ar-$H_{2,6}$), 7.43–7.38 (3H, m, H_{13} and Ar-$H_{3,5}$), 3.22 (3H, s, CH_3, H_7); ^{13}C NMR (100.63 MHZ, DMSO-d_6) δ_C/ppm: 20.49 (C_7), 119.83 (C_{11}), 120.09 (C_2, C_6), 121.13 (C_8), 123.25 (C_{13}), 130.14 (C_3, C_5), 134.26 (C_4), 137.31 (C_{12}), 138.49 (C_1), 148.80 (C_9), 149.33 (C_{14}), 149.54 (C_{10}). These assignments were confirmed using DEPT ^{13}C (135°), ^1H–^1H COSY and ^1H–^{13}CHMQC two-dimensional correlation spectroscopy. HRMS TOF (ESI+) (water:acetonitrile = 1:3) with the highest molecular weight ion peak matching, was at m/z = 571.1129 (80%) and is related to $[[Zn(L^2)_2Cl_2]-Cl]^+$. The calculated value for $[(C_{28}H_{24}N_8ZnCl)]^+$ is 571.1104. Λ_M(DMSO) = 8 $\Omega^{-1}\ cm^2\ mol^{-1}$. Elemental *Anal.* Calc. for $C_{28}H_{24}N_8Cl_2Zn$: C, 55.2; H, 4.0; N, 18.4. Found: C, 55.4; H, 3.8;

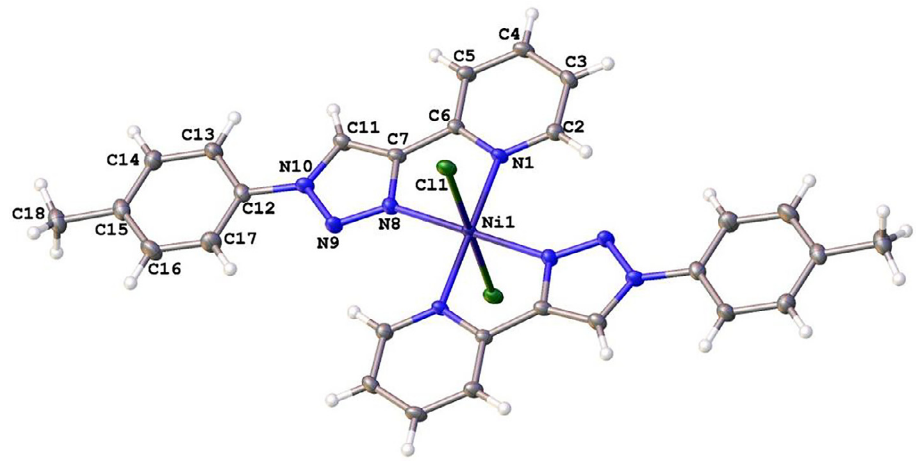

Fig. 3. View of $[Ni(L^2)_2Cl_2]$ showing the atom labelling scheme. The asymmetric unit contains one ligand, one Cl and the Ni atom which lies on an inversion centre, the second ligand and Cl atom are generated by symmetry (−*x*, 1−*y*, 1−*z*). Displacement ellipsoids for non-hydrogen atoms are drawn at 50% probability level.

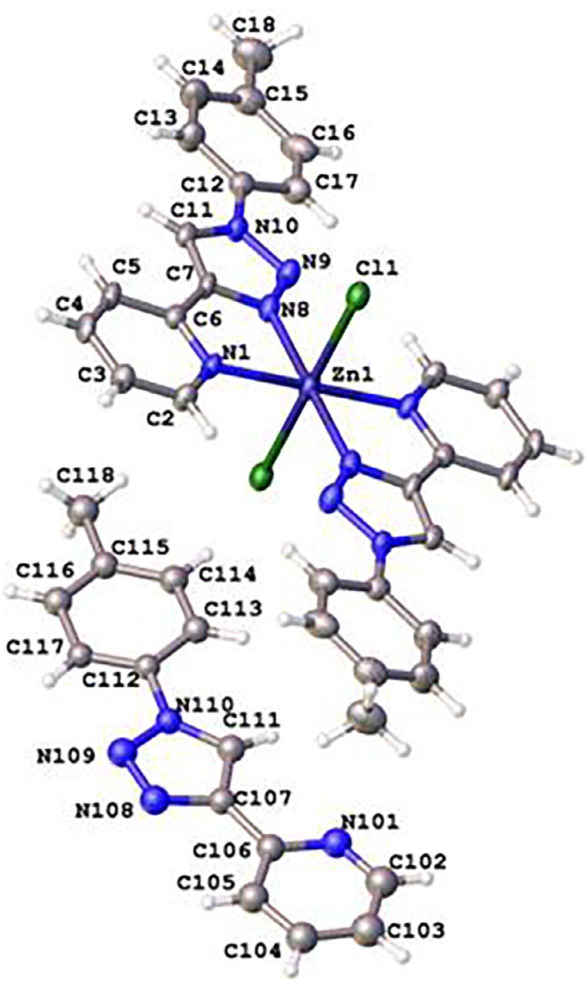

Fig. 4. View showing atom labelling scheme of $[Zn(L^2)_2Cl_2]{\cdot}L^2$. Displacement ellipsoids for the atoms refined with anisotropic adps and spheres for those with isotropic adps are drawn at 50% probability level. The asymmetric unit contains one coordinated ligand, one Cl and the Zn which lies on an inversion centre and 0.5 free ligand molecule. The free ligand molecule is disordered over an inversion centre and the second orientation is omitted for clarity.

N, 18.2%. A good single crystal of $[Zn(L^2)_2Cl_2]{\cdot}L^2$ for X-ray structural analysis was obtained by slow evaporation of a hot CH_3OH solution of the $[Zn(L^2)_2Cl_2]$.

*2.2.7. Dichloro(bis{2-[1-(4-methylphenyl)-1H-1,2,3-triazol-4-yl-κN^3] pyridine-κN})cadmium(II) (**7**)*

For the preparation of $[Cd(L^2)_2Cl_2]$, the method used was as described for that of the $[Mn(L^2)_2Cl_2]$. An amount of anhydrous $CdCl_2$ of 0.15 g, 0.82 mmol and 0.39 g, 1.65 mmol of L^2 were used, and an identical work-up procedure gave the required compound as a white solid, and the isolated precipitate gave (0.18 g, 0.27 mmol, yield 78%), mp. 306–308 °C. ATR/IR: $\overline{\nu}(cm^{-1})$; 3102, 1624, 1603, 1572, 1521, 1469, 1449, 1264, 1239, 1062, 1015, 1004, 815, 781, 749, 720. UV–Vis (DMSO) λ_{max}: $[Cd(L^2)_2Cl_2]$ showed absorption bands at 256 nm, ε_{max} = 33 448 $dm^3\ mol^{-1}\ cm^{-1}$, 260 nm, ε_{max} = 31 724 $dm^3\ mol^{-1}\ cm^{-1}$, 287 nm, ε_{max} = 29 655 $dm^3\ mol^{-1}\ cm^{-1}$. NMR data (ppm), δ_H (400 MHZ, DMSO-d_6): 9.26 (1H, s, H_8), 8.66–8.67 (1H,d, J_{HH} = 4.12 Hz, H_{14}), 8.11–8.10 (1H, dd, $^1J_{HH}$ = 7.73 Hz, H_{11}), 7.98–7.95 (1H, dt, $^1J_{HH}$ = 7.79 Hz, $^2J_{HH}$ = 1.83 Hz, H_{12}), 7.89–7.87 (2H,d, J_{HH} = 8.24 Hz, Ar-$H_{2,6}$), 7.43–7.41 (3H, m, H_{13} and Ar-$H_{3,5}$), 3.23 (3H, s, CH_3); ^{13}C NMR (100.63 MHZ, DMSO-d_6) δ_C/ppm: 20.50 (C_7), 119.98 (C_{11}), 120.12 (C_2, C_6), 121.27 (C_8), 123.39 (C_{13}), 130.17 (C_3, C_5), 134.23 (C_4), 137.52 (C_{12}), 138.58 (C_1), 148.47 (C_9), 148.97 (C_{14}), 149.50 (C_{10}). These assignments were confirmed using DEPT ^{13}C (135°), ^1H–^1H COSY and ^1H–^{13}C HMQC two-dimensional correlation spectroscopy. HRMS TOF (ESI+) (water:acetonitrile = 1:3) with the highest molecular weight ion peak matching, was observed at *m*/*z* = 621.0856 (100%) and is assigned to $[[Cd(L^2)_2Cl_2]{-}Cl]^+$ The calculated value for $[(C_{28}H_{24}N_8CdCl)]^+$ is 621.0846. Λ_M (DMSO) = 16 $\Omega^{-1}\ cm^2\ mol^{-1}$. Elemental *Anal.* Calc. for $C_{28}H_{24}N_8Cl_2Cd$: C, 51.3; H, 3.7; N, 17.1. Found: C, 51.3; H, 3.8; N, 17.3%.

2.3. Instruments and measurement parameters

Infrared (ATR-FTIR IR) spectra were recorded using a smart diamond ATR attachment on a Thermo-Nicolet FT-IR Spectrometer (AVATAR 320) over the range 4000 to 400 cm^{-1}. Mass spectra were performed at the EPSRC Mass Spectrometry Service Centre, University of Wales, Swansea and University of Sheffield. The instrument used was the 'WATERS LCT premier', the ionization was electrospray (ESI+), the solvent was water/acetonitrile (1:3), while the ionization was electrospray (ESI+ and ES−). Thermofisher LTQ Orbitrap XL was used to analyse volatile molecules in the mass range *m*/*z* 50–2000 or *m*/*z* 200–4000 Daltons. NMR spectra (^1H, ^{13}C, COSY, ^{13}C–^1H correlated NMR) were recorded on a ECS-400 MHz, JEOL multi nuclear FT spectrometer, using Optiplex 380 Delta 5.02 software, with tetramethylsilane (TMS) as an internal standard for ^1H NMR analysis. Chemical shifts were reported in ppm downfield from

Table 1
IR frequencies in wavenumber (cm^{-1}) units of the ligand (L^2) and the $[M(L^2)_2Cl_2]$ coordination compounds.

Compound	ν (C=N)$_{pyridine}$, ν(C=C)$_{Ar}$, ν(C=N)$_{triazole}$	ν(C=C)$_{triazole}$	ν (N–N)$_{triazole}$, ν(N=N)$_{triazole}$	ν(C–N)
L^2	1597, 1592, 1566	1543	1144, 1036	1517
$[Mn(L^2)_2Cl_2]$ (**1**)	1606, 1595, 1575	1556	1157, 1062	1521
$[Fe(L^2)_2Cl_2]$ (**2**)	1605, 1595, 1571	1555	1152, 1063	1522
$[Co(L^2)_2Cl_2]$ (**3**)	1609, 1595, 1575	1554	1152, 1065	1522
$[Ni(L^2)_2Cl_2]$ (**4**)	1612, 1596, 1577	1566	1152, 1067	1521
$[Cu(L^2)_2Cl_2]$ (**5**)	1606, 1594, 1575	1556	1156, 1063	1516
$[Zn(L^2)_2Cl_2]$ (**6**)	1607, –, 1570	1549	1153, 1055	1517
$[Cd(L^2)_2Cl_2]$ (**7**)	1624, 1603, 1572	1564	1156, 1062	1521

Table 2
Crystallographic data for the $[Ni(L^2)_2Cl_2]$ and $[Zn(L^2)_2Cl_2]\cdot L^2$.

Compound	$[Ni(L^2)_2Cl_2]$	$[Zn(L^2)_2Cl_2]\cdot L^2$
Empirical formula	$C_{28}H_{24}Cl_2N_8Ni$	$C_{42}H_{36}Cl_2N_{12}Zn$
Formula weight	602.16	845.1
T (K)	293(2)	100(2)
λ (Å)	0.71075	0.71075
Crystal system	monoclinic	monoclinic
Space group	$P2_1/c$	$P2_1/c$
Unit cell dimensions		
a (Å)	10.7323(7)	15.279(8)
b (Å)	12.9118(7)	12.919(6)
c (Å)	9.7218(5)	9.866(5)
α (°)	90	90
β (°)	104.686(7)	102.528(6)
γ (°)	90	90
V (Å^3)	1303.17(13)	1901.1(16)
Z	2	2
ρ (Mg/m^3)	1.535	1.476
μ (mm^{-1})	0.985	0.837
$F(000)$	620	872
Crystal	plate; colourless	plate; colourless
Crystal size (mm^3)	$0.09 \times 0.04 \times 0.01$	$0.07 \times 0.04 \times 0.01$
θ (°)	3.16–27.47	2.64–27.51
Index ranges	$-13 \le h \le 10$, $-16 \le k \le 16$, $-12 \le l \le 12$	$-19 \le h \le 19$, $-16 \le k \le 16$, $-12 \le l \le 12$
Reflections collected	8726	16822
Independent reflections (R_{int})	2969 (0.039)	4328 (0.075)
Completeness to θ = 27.47°	99.20%	99.20%
Absorption correction	semi-empirical from equivalents	semi-empirical from equivalents
Maximum and minimum transmission	1.000 and 0.675	1.000 and 0.733
Refinement method	full-matrix least-squares on F^2	full-matrix least-squares on F^2
Data/restraints/parameters	2969/0/179	4328/0/252
Goodness-of-fit (GOF) on F^2	1.02	1.20
Final R indices [$F^2 > 2\sigma(F^2)$]	R_1 = 0.040, wR_2 = 0.087	R_1 = 0.087, wR_2 = 0.158
R indices (all data)	R_1 = 0.057, wR_2 = 0.094	R_1 = 0.113, wR_2 = 0.171
Largest difference in peak and hole (e Å^{-3})	0.56 and −0.54	0.46 and −0.72

tetramethylsilane (TMS), at 298 K, with coupling constants (J) reported in Hertz (Hz). Standard abbreviations indicating multiplicity were used as follows: m = multiplet, t = triplet, d = doublet and s = singlet. UV–Vis spectra were obtained on a Perkin Elmer Lambda 40 UV/Vis spectrometer. Magnetic susceptibility is measured with a Gouy magnetic susceptibility balance. The gram magnetic susceptibility for a substance is calculated from:

$$\chi_g = (C_{bal})(l)(R - R_o)/(10^9)(m)$$

where l = height of sample in the tube in units of centimeters, m = mass of the sample in units of grams, R = reading for tube plus sample, R_o = reading for the empty tube and C_{bal} = balance calibration constant = 1.0. The molar magnetic susceptibility is then calculated from the gram magnetic susceptibility using the following equation.

$$\chi_m = (\chi_g)(\text{molar mass})$$

The effective magnetic moment for a particular substance is calculated from the molar magnetic susceptibility [8] using the following equation (T represents the Kelvin temperature (294 K)):

$$\mu_{eff} = 2.83[(\chi_m)(T)]^{1/2}$$

The calculated μ_{eff} values for the $[M(L^2)_2Cl_2]$ coordination compounds are given in the experimental characterization data.

2.4. X-ray diffraction

Single crystal X-ray diffraction measurements for $[Ni(L^2)_2Cl_2]$ and $[Zn(L^2)_2Cl_2]\cdot L^2$ were performed using a Rigaku SPIDER RAXIS image plate detector and Rigaku AFC12 goniometer equipped with an enhanced sensitivity (HG) Saturn724+ detector mounted at the window of an FR-E+ SuperBright molybdenum rotating anode generator with HF Varimax optics (100 μm focus) respectively.

Data were processed and empirical absorption corrections were carried out using Crystal Clear SM-Expert [9]. The structures were solved by direct methods using SHELXS-97 within OLEX2 [10]. All refinements on F_o^2 by full-matrix least squares refinement were performed using the SHELXL-97 program package within OLEX2 [11]. All non-hydrogen atoms for the Zn coordination compound were refined with anisotropic displacement parameters however the free ligand is disordered over an inversion centre and was modelled as 0.5 occupied with isotropic displacement parameters. No distance restraints were applied or required. Hydrogen atoms were added at calculated positions and included as part of a riding model with C—H (aromatic) 0.93 Å $U_{ISO} = 1.2U_{eq}$ (C); C—H (methyl) 0.96 Å $U_{ISO} = 1.5U_{eq}$ (C). Perspective drawings [11] of the molecular structure of $[Ni(L^2)_2Cl_2]$ and $[Zn(L^2)_2Cl_2]{\cdot}L^2$, also showing the atom numbering scheme used, are shown in Figs. 3 and 4. Crystallographic data are presented in Table 2 with selected bond lengths, bond angles and torsion angles in Table 3.

2.5. Theoretical approach

Density functional theory (DFT) calculations were performed with the B3LYP functional as implemented in the Gaussian 09 package [12] using the triple-ζ basis set 6-311G(d,p), except for Cd where the Stuttgart/Dresden (SDD) pseudopotential was used to describe the metal electronic core, while the metal valence electrons were described using the def2-TZVPP basis set [13]. Since the coordination compounds of this study are paramagnetic, all the different spin states were considered when performing the DFT calculations. Calculations were done spin unrestricted in the gas phase. All structures were confirmed as true minimum structures by a frequency analysis, i.e. no imaginary frequencies. The input coordinates for the molecules were constructed using Chemcraft [14]. Natural bond orbital (NBO) analysis (using the NBO 3.1 module [15] in Gaussian 09), as well as an electronic density analysis (using Bader's quantum theory of atoms in molecules (QTAIM) [16–18], as implemented in ADF2017 [19–21]) were performed on an optimized structure of two $[Zn(L^2)_2Cl_2]$ molecules. The input coordinates for the latter were obtained from the crystal data, also presented in this study.

3. Results and discussion

3.1. Characterization

The dichloro(bis{2-(1-(4-methylphenyl)-1H-1,2,3-triazol-1-yl) pyridine}-metal coordination compounds $[M(L^2)_2Cl_2]$, were synthesized from a 2:1 mol ratio of 2-(1-(4-methyl-phenyl)-1H-1,2,3-triazol-1-yl)pyridine and the metal chloride. These compounds were characterized by FT-IR, MS, elemental analysis, NMR (Zn and Cd), UV–Vis, melting points, magnetic moments, conductivity measurements, single crystal X-ray diffraction (Ni and Zn) and computational chemistry calculations.

Comparison of the IR spectra of the $[M(L^2)_2Cl_2]$ coordination compounds with that of the 2-(1-(4-methyl-phenyl)-1H-1,2,3-triazol-1-yl)pyridine ligand (L^2), shows that characteristic bands were shifted due to complex formation (see Table 1). For example, ν (C=N) stretching band of the pyridine moiety is observed at a value around 1624–1606 cm^{-1} for the various $[M(L^2)_2Cl_2]$ coordination compounds, which is shifted to higher wavenumbers than in the free ligand (1597 cm^{-1}). This indicates coordination of the nitrogen of the C=N pyridine moiety to the different metal atoms. The region for $\nu(C{=}C)_{Ar}$ bands of phenyl ring in complexes, are around ν = 1598–1580 cm^{-1} and 1500–1470 cm^{-1} [22,23]. The $\nu(C{=}N)_{\boldsymbol{triazole}}$ absorption band of the triazole moiety at 1566 cm^{-1} in the free ligand is detected around 1570–1577 cm^{-1} in the $[M(L^2)_2Cl_2]$

Table 3
Selected bond lengths (Å) and bond angles (°) for the $[Ni(L^2)_2Cl_2]$ and $[Zn(L^2)_2Cl_2]{\cdot}L^2$.

	$[Ni(L^2)_2Cl_2]$	$[Zn(L^2)_2Cl_2]{\cdot}L^2$
Bond distance (Å)		
M1—N1	2.1015(19)	2.144(3)
M1—N8	2.0739(19)	2.191(4)
M1—Cl1	2.4123(6)	2.4615(14)
N1—C2	1.341(3)	1.341(5)
N1—C6	1.352(3)	1.346(5)
N8—N9	1.316(3)	1.316(5)
N8—C7	1.357(3)	1.363(5)
N9—N10	1.352(3)	1.364(5)
N10—C11	1.353(3)	1.352(5)
N10—C12	1.428(3)	1.434(5)
Bond angle (°)		
N8^i—M1—N8	180	180
N8—M1—N1^i	100.41(8)	77.78(13)
N8—M1—N1	79.59(8)	102.22(13)
N1i—M1—N1	180	180
Cl1—M1—Cl1i	180	180
C2—N1—C6	117.9(2)	119.0(4)
C2—N1—M1	127.46(16)	125.5(3)
C6—N1—M1	114.55(15)	115.4(3)

Symmetry transformations used to generate equivalent atoms: (i) $-x + 1$, $-y + 1$, $-z + 1$ for $[Ni(L^2)_2Cl_2]$ and (i) $-x$, $-y + 1$, $-z + 1$ for $[Zn(L^2)_2Cl_2]{\cdot}L^2$.

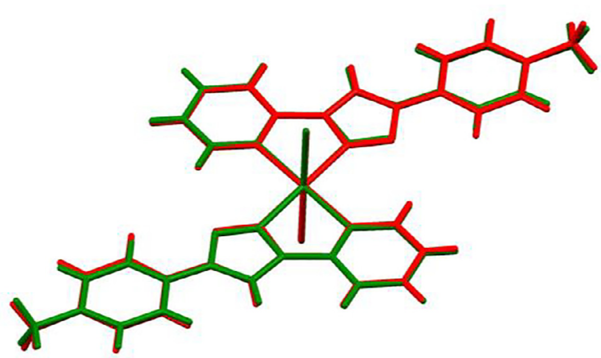

Fig. 5. Overlay $[Ni(L^2)_2Cl_2]$ (red) and $[Zn(L^2)_2Cl_2]$ (green). The root means square (RMS) overlay values, when using the metal and the six atoms of the octahedral coordination polyhedron, is 0.078. (Colour online.)

coordination compounds, while the $\nu(C{=}C)_{\boldsymbol{triazole}}$ absorption band of the triazole moieties which appear at 1543 cm^{-1} in the free ligand is detected around 1549–1566 cm^{-1} in the $[M(L^2)_2Cl_2]$ coordination compounds, as indicated in Table 1.

The experimentally measured room temperature magnetic moment for the paramagnetic $[M(L^2)_2Cl_2]$ coordination compounds (**1**)–(**4**) of this study are consistent with high spin complexes, namely Mn (μ_{eff} = 5.62 B.M., S = 5/2), Fe (μ_{eff} = 5.26 B.M., S = 2), Co (μ_{eff} = 3.98 B.M., S = 3/2), Ni (μ_{eff} = 3.00 B.M., S = 1), while $[Cu(L^2)_2Cl_2]$ (**5**) (μ_{eff} = 1.70 B.M., S = ½) can only be low spin. The molar conductivity measurements of the $[M(L^2)_2Cl_2]$ coordination compounds were conducted using 10^{-3} M solutions of $[M(L^2)_2Cl_2]$ in DMSO. The molar conductivities ranged from 6 to 50 Ω^{-1} cm^2 mol^{-1} at 294 K. The low values indicate that the chloride anions bind to the metal ions as coligands and do not ionize. Low conductivity values are indicative of coordination compounds having 1:2 metals:ligand stoichiometry of the type ML_2Cl_2, where L acts as a bidentate ligand [24]. Higher than expected conductivity values are usually due to the possible displacement of one chlorine atom by one molecule of the solvent DMSO in the $[M(L^2)_2Cl_2]$ coordination compounds, producing intermediate behaviour $[ML_2(Cl)(DMSO)]{\cdot}Cl$ between those of non-electrolytes and 1:1 electrolytes. Similar behaviours were observed for several coordination compounds, mainly measured in DMSO as solvent, because this solvent

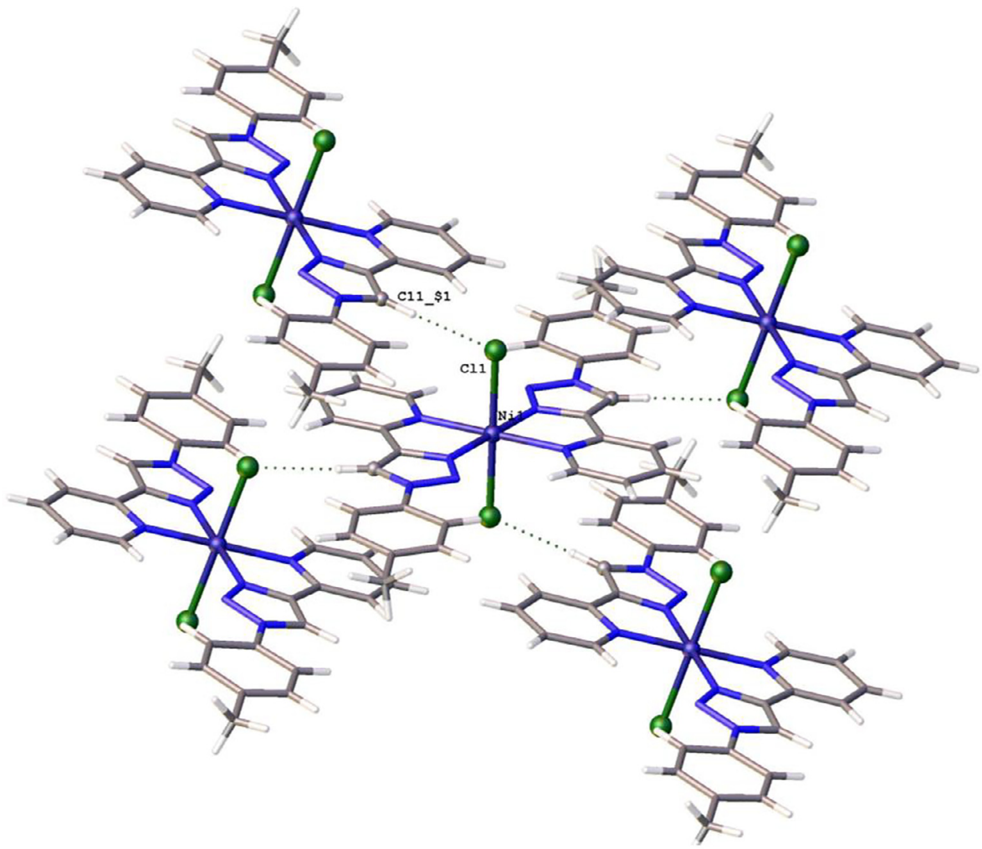

Fig. 6. Partial packing for $[Ni(L^2)_2Cl_2]$ showing an intermolecular C—H···Cl hydrogen bonding interaction between Cl1…H11_$1-C11_$1; Cl1…H11_$1 2.44 Å, Cl1_C11_$1 3.366 Å and the angle C11_$1-H11_41…Cl1 is 174.2°, $1 signifies symmetry code *1−x, ½−y, 3/2−z.*

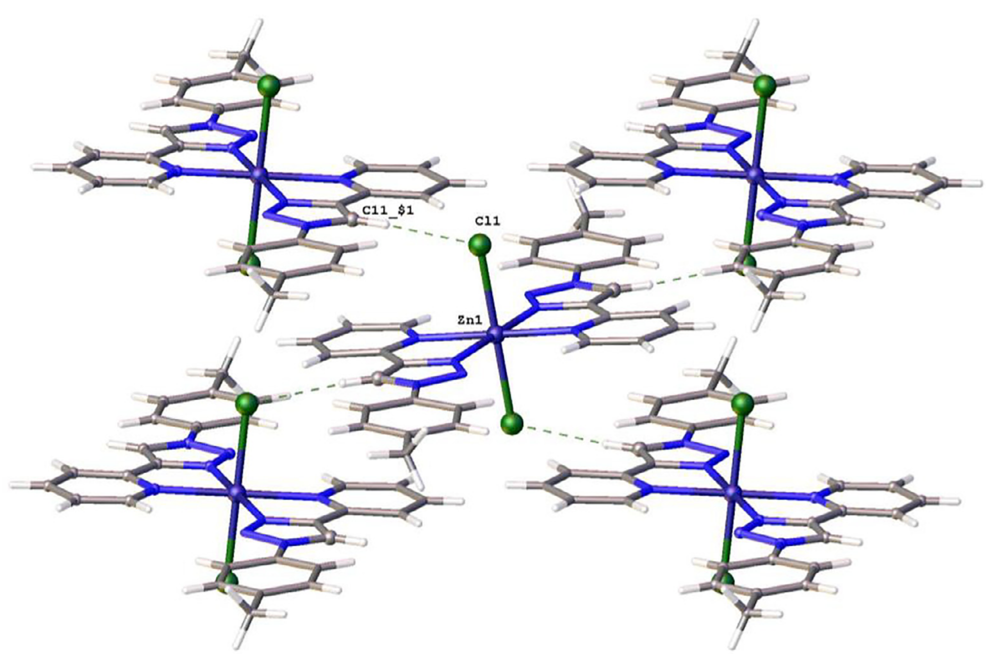

Fig. 7. Partial packing for $[Zn(L^2)_2Cl_2]{\cdot}L^2$ showing (Intermolecular C—H…Cl hydrogen bonding interaction between Cl1…H11_$1-C11_$1; Cl1…H11_$1 2.55 Å, Cl1_C11_$1 3.473 Å and the angle C11_$1-H11_41…Cl1 is 170.1°, $1 signifies symmetry code *x, 3/2−y, −1/2 + z).*

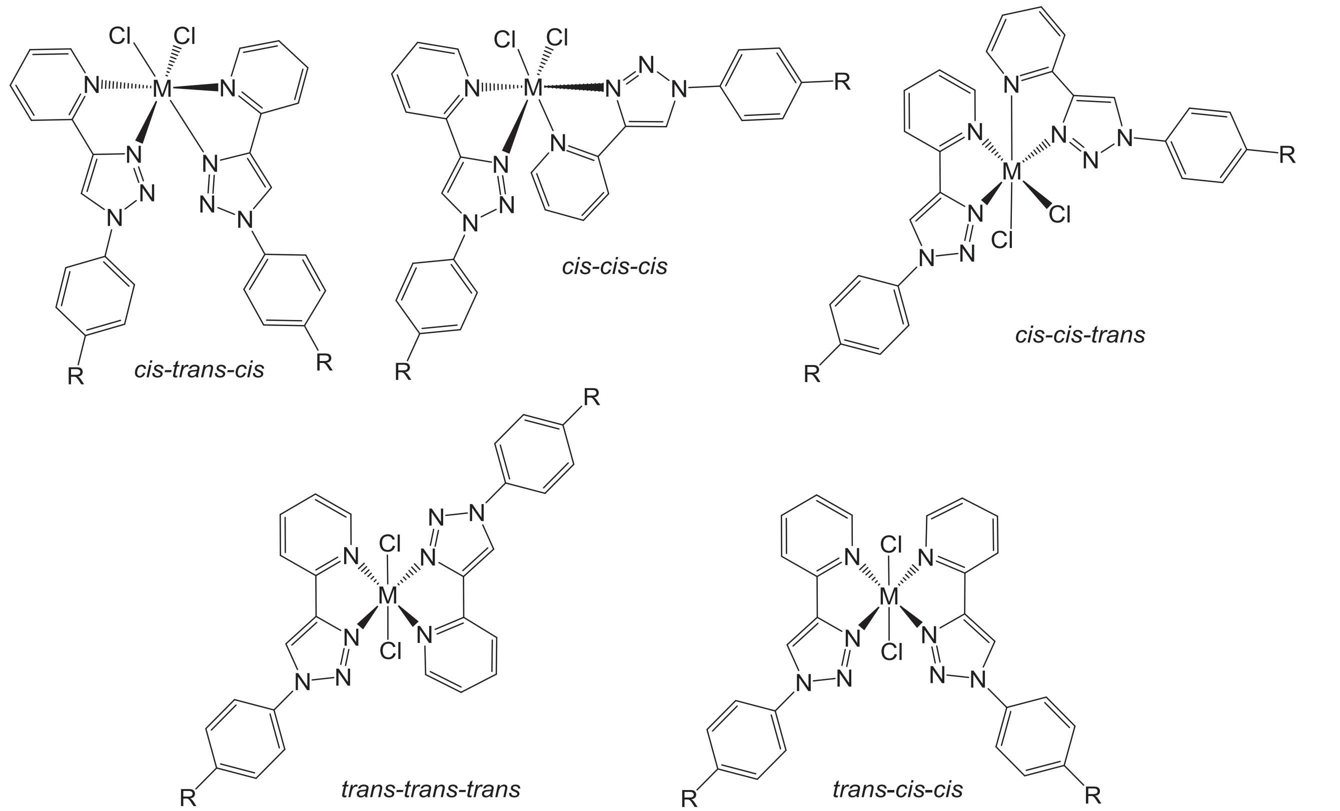

Fig. 8. Geometrical isomers for [ML_2Cl_2] coordination compounds. R = CH_3 for coordination compounds 1–9 of this study. The isomers are defined by the relative orientation of the Cl, N_{Py} and $N_{triazole}$ molecules around the metal respectively. R = H for the unsubstituted ligand, L^1, R = CH_3 for the CH_3 substituted ligand, L^2, and R = OCH_3 for the OCH_3 substituted ligand, L^3.

is a strong donor with profitable steric properties [25,26]. The ^{13}C and ^{1}H NMR spectra of [$Zn(L^2)_2Cl_2$] (**6**) and [$Cd(L^2)_2Cl_2$] (**7**) show no impurities, including no traces of the ligand L^2.

3.2. X-ray structures

The molecular structure of the coordination compounds [$Ni(L^2)_2Cl_2$] and [$Zn(L^2)_2Cl_2$]·L^2 are presented here. Perspective drawings of the molecular structures, also showing the atom numbering schemes, are given in Fig. 3 for [$Ni(L^2)_2Cl_2$] and Fig. 4 for [$Zn(L^2)_2Cl_2$]·L^2. Crystallographic data are given in Table 2 with selected bond lengths and bond angles in Table 3. The structures can be described as *trans–trans–trans*, since the Cl, N_{Py} and $N_{triazole}$ are orientated *trans* to each other respectively in [$Ni(L^2)_2Cl_2$] and [$Zn(L^2)_2Cl_2$]·L^2. A *trans–trans–trans* isomer was also previously found for [$Ni(L)_2Br_2$] with L = 2-[1-(4-cyclohexyl)-1H-1,2,3-triazol-4-yl]pyridine [4]. Both [$Ni(L^2)_2Cl_2$] and [$Zn(L^2)_2Cl_2$]·L^2 crystallized in the $P2_1/c$ space group with the metal centre lying on an inversion symmetry. However, a free ligand L^2, crystallized in a 1:1 ratio with [$Zn(L^2)_2Cl_2$]. The structures of the molecules [$Ni(L^2)_2Cl_2$] and [$Zn(L^2)_2Cl_2$]·L^2 are very similar as can be seen from the overlay of the two structures in Fig. 5. The bond lengths and angles of the two structures differ very slightly, see data in Table 3.

Intermolecular H-bonding interaction involving the chloride atoms in [$Ni(L^2)_2Cl_2$] form a 3D supramolecular structure [27] [28], see Fig. 6. The zinc structure is different as it contains molecules of the free ligand L^2 and [$Zn(L^2)_2Cl_2$] molecules. The molecules in the layers of the [$Zn(L^2)_2Cl_2$]·L^2 structure are also held together by hydrogen bonds, see Fig. 7. The intermolecular separations suggest there are hydrogen bonds between both the coordinated and free ligand and between free ligand molecules but are not analysed further given the disordered nature of the free ligand.

3.3. DFT study

The relative orientation of the Cl, N_{Py} and $N_{triazole}$ molecules around the metal respectively, in each of 1–7, can lead to five geometrical isomers, namely *cis–trans–cis*, *cis–cis–cis*, *cis–cis–trans*, *trans–trans–trans*, and *trans–cis–cis*, as shown in Fig. 8. DFT calculations on the different isomers and possible spin states of the series of [$M(L^1)_2Cl_2$] coordination compounds, L^1 with R = H (Fig. 2) and M = Mn (1), Fe (2), Co (3), Ni (4), Cu (5), Zn (6) and Cd (7), confirmed the experimentally measured spin states for 1–7, see Table 4. Thus, d^5 Mn(II) (with μ_{eff} = 5.62 B.M., S = 5/2), d^6 Fe(II) (with μ_{eff} = 5.26 B.M., S = 2), d^7 Co(II) (with μ_{eff} = 3.98 B.M., S = 3/2), d^8 Ni(II) (with μ_{eff} = 3.00 B.M., S = 1), d^9 Cu(II) (with μ_{eff} = 1.70 B.M., S = ½), are all paramagnetic, while d^{10} Zn(II) and Cd(II) are diamagnetic with S = 0.

Since the *cis–cis–trans* and the *trans–trans–trans* isomers for the [$M(L^1)_2Cl_2$] coordination compounds, both with N_{Py} *trans* to each other, are generally equi-energetic within 0.15 eV, both isomers could experimentally be possible. In Table 5 DFT calculations for the lowest energy spin state of each isomer of the dichloro{bis[2-(1-(4-methylphenyl)-1H-1,2,3-triazol-4-yl-κN^3]pyridine-κN]} metal(II), [$M(L^2)_2Cl_2$], with a methyl substituent on the phenyl ring (L^2 = 2-(1-(4-methylphenyl)-1H-[1,2,3-triazol]-4-yl)pyridine), are given.

In this study, the *trans–trans–trans* isomer was obtained both for [$Ni(L^2)_2Cl_2$], **4**, and [$Zn(L^2)_2Cl_2$], **6**. Only in one case a *cis–cis–trans* isomer for this kind of coordination compounds was obtained till date [29], namely for *cis–cis–trans* [$Mn(L^3)_2Cl_2$], L^3 with R = OCH_3 (Fig. 2) [6], while *trans–trans–trans* isomers were reported for [$Ni(L)_2Br_2$] [4], [$Co(L^3)_2Cl_2$] [6] and [$Ni(L^3)_2Cl_2$] [6].

To shed more light on the experimental observation that the *trans–trans–trans* isomers are generally experimentally favoured

Table 4
Relative Electronic energies E (eV) for the indicated spin states and geometrical isomers of $[M(L^1)_2Cl_2]$, containing L^1 with R = H (Fig. 2). The energy of the lowest energy isomer is indicated in bolt font.

Isomer[a]	S	E (eV) Mn[b]	E (eV) Co[b]	E (eV) Cu	S	E (eV) Fe	E (eV) Ni[b]	E (eV) Zn	E (eV) Cd
ctc	1/2	1.90	1.07	0.33	0	1.11	1.20	0.40	0.29
ccc		1.69	0.80	0.35		0.88	1.21	0.21	0.12[e]
cct		1.49	0.71	0.15		0.63	0.97	**0.00**	**0.00**
ttt		1.35	0.56	**0.00**		0.61	0.93	**0.11**	**0.15**
tcc		1.64	0.74	0.20		0.89	1.11	0.28	[d]
ctc	3/2	1.78	0.45	–	1	1.18	0.50	–	–
ccc		[c]	0.24	–		0.97	0.29	–	–
cct		[c]	**0.04**	–		0.78	**0.06**	–	–
ttt		2.19	**0.00**	–		1.95	**0.00**	–	–
tcc		1.64	0.22	–		0.91	0.25	–	–
ctc	5/2	0.33	–	–	2	0.48	–	–	–
ccc		0.17	–	–		0.27	–	–	–
cct		**0.00**	–	–		**0.10**	–	–	–
ttt		**0.14**	–	–		**0.00**	–	–	–
tcc		[d]	–	–		0.19	–	–	–

[a] See Fig. 8 for the geometry of the different isomers.
[b] From Ref. [6].
[c] Geometry did not converge.
[d] Optimized to the *cct* isomer.
[e] Optimized to a 5-coordinated coordination compound, not 6-coordinated.

Table 5
Relative electronic energies *E* (eV) for the indicated spin states and geometrical isomers of $[M(L^2)_2Cl_2]$, containing L^2 with R = CH_3 (Fig. 2). The energy of the lowest energy isomers are indicated in bolt font.

Isomer[a]	*E* (eV) Mn *S* = 5/2	*E* (eV) Fe *S* = 4/2	*E* (eV) Co *S* = 3/2	*E* (eV) Ni *S* = 1	*E* (eV) Cu *S* = 1/2	*E* (eV) Zn *S* = 0	*E* (eV) Cd *S* = 0
ctc	0.33	0.48	0.48	0.51	0.33	0.39	0.28
ccc	0.17	0.27	0.24	0.25	0.35	0.20	0.12[b]
cct	**0.00**	**0.10**	**0.04**	**0.06**	**0.15**	**0.00**	**0.00**
ttt	**0.14**	**0.00**	**0.00**	**0.00**	**0.00**	**0.11**	**0.15**
tcc	[a]	0.20	0.23	0.26	0.20	0.28	[a]

[a] Optimized to the *cct* isomer.
[b] Optimized to a 5-coordinated coordination compound, not 6-coordinated.

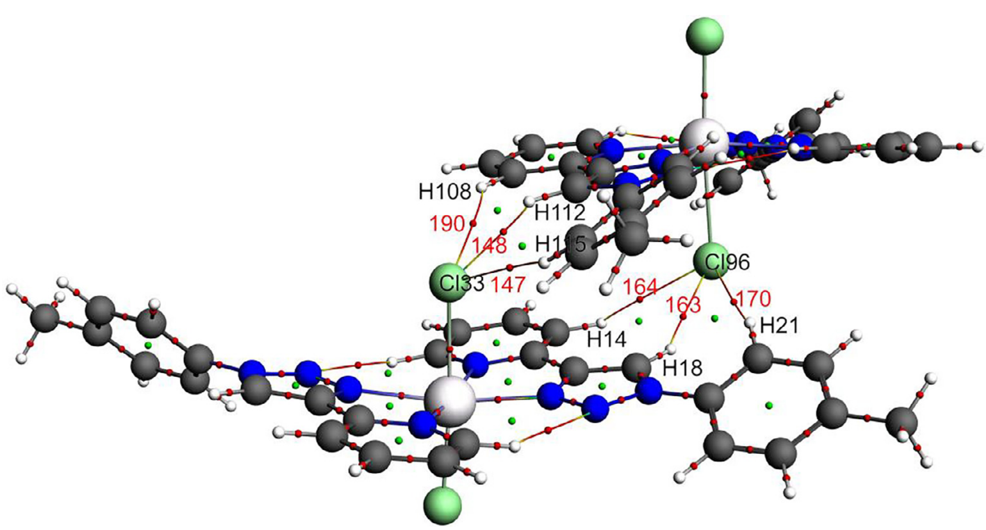

Fig. 9. Visualization of the optimized di-molecular model of $[Zn(L^2)_2Cl_2]$, showing bond-paths (BP) coloured according to the value of the electron density; blue (high density) to green to red (low density). Bond critical point (BCP) numbers, related to inter-molecular bonds, are indicated in red font. Colour code of atoms (online version): Zn (off-white), C (grey), N (blue), Cl (green), H (white). (Colour online.)

for metal(II)-(1,2,3-triazol-4-yl)pyridine coordination compounds, although DFT calculations predict that both the *cis–cis–trans* and the *trans–trans–trans* isomers could experimentally be possible, we present here results for a di-molecular model of $[Zn(L^2)_2Cl_2]$, where two $[Zn(L^2)_2Cl_2]$ molecules were optimized together. The resulting optimized di-molecular structure was evaluated by Bader's quantum theory of atoms in molecules (QTAIM) method, as well as by the Weinhold natural bonding orbital (NBO) method

Table 6
Selected QTAIM calculated topological parameters related to the intermolecular hydrogen bonds in the optimized di-molecular model of $[Zn(L^2)_2Cl_2]$ shown in Fig. 9.

BCP	Atoms involved	Inter-atomic distance /Å	BP length /Å	Electron density ρ/e a_0^{-3}	Laplacian of electron density $\nabla^2\rho$/e a_0^{-5}
CP # 190	Cl33–H108	3.056	3.077	0.0051	0.0156
CP # 148	Cl33–H112	2.425	2.443	0.0171	0.0510
CP # 147	Cl33–H115	2.867	2.875	0.0072	0.0220
CP # 170	Cl96–H21	2.907	2.917	0.0067	0.0205
CP # 163	Cl96–H18	2.427	2.446	0.0170	0.0508
CP # 164	Cl96–H14	2.999	3.018	0.0057	0.0174

to evaluate the nature of the intermolecular hydrogen bonds between chlorine and H-atoms by theoretical computational chemistry methods. Bader's definition of an atom in a molecular system, is based purely on the electronic charge density, while zero flux surfaces divide atoms. The position the nuclei of atoms, an atom critical point, ACP (3, −3), is determined by a local maximum of electron density, with the electron density decreasing in all three perpendicular directions of space. The atoms are connected by bond paths with a bond critical point, BCP (3, −1), along the bond where the shared electron density reaches a minimum [30]. QTAIM calculated electron density at H-bond critical points correlates well with experimental hydrogen bond strengths [31–33]. Typical calculated topological parameters for hydrogen-bonds, i.e. X—H···Y through-space interactions, are 0.002–0.04 au for the electron density and 0.02–0.15 au for the Laplacian of the electron density [34,35] at the H···Y BCP. The inter-molecular bond paths identified for the optimized di-molecular model of $[Zn(L^2)_2Cl_2]$, are shown in Fig. 9 with the related topological parameters summarized in Table 6. All QTAIM calculated inter-molecular bonds are C—H···Cl bonds with electron density and Laplacian of the electron density values that fall within the typical values for hydrogen bonds. The shortest and strongest QTAIM identified inter-molecular C—H···Cl bonds numbered 148 and 163 in Fig. 9, are the same as experimental observed for $[Zn(L^2)_2Cl_2]$ as shown in Fig. 7.

The Weinhold NBO method can be used to describe intermolecular interactions from a natural bond orbital, donor–acceptor viewpoint. In the optimized di-molecular model of $[Zn(L^2)_2Cl_2]$, a lone pair on Cl acts as donor to donate electron density into an empty antibonding orbital of nearby C—H as acceptors. Nine LP(Cl33) → BD*(C—H) from Cl33 to the three nearest hydrogens (H108, H112 and H115) as shown in Fig. 10 and tabulated in Table 7, are identified by the NBO calculation. The LP(3) (Cl33) → BD*(1) (C111–H112) donor–acceptor interaction of 14.853 kJ·mol^{-1} is the strongest, and is the same as the experimental C—H...Cl hydrogen bonding interaction observed in the solid state for $[Zn(L^2)_2Cl_2]$ as shown in Fig. 7. Due to symmetry, nine similar LP(Cl96) → BD*(C—H) from Cl 96 to the three nearest hydrogens (H14, H18 and H21) exist (not shown in Fig. 10, values tabulated in Table 7). The theoretically obtained donor–acceptor interaction from a filled lone pair NBO on Cl to an empty antibonding NBO on (C—H), and the QTAIM determined bonding paths between Cl and nearby hydrogens on a neighboring molecule, thus give an understanding on a molecular level, why in the solid state where inter-molecular forces and packing play a role, the *trans–trans–trans* isomers are mostly obtained.

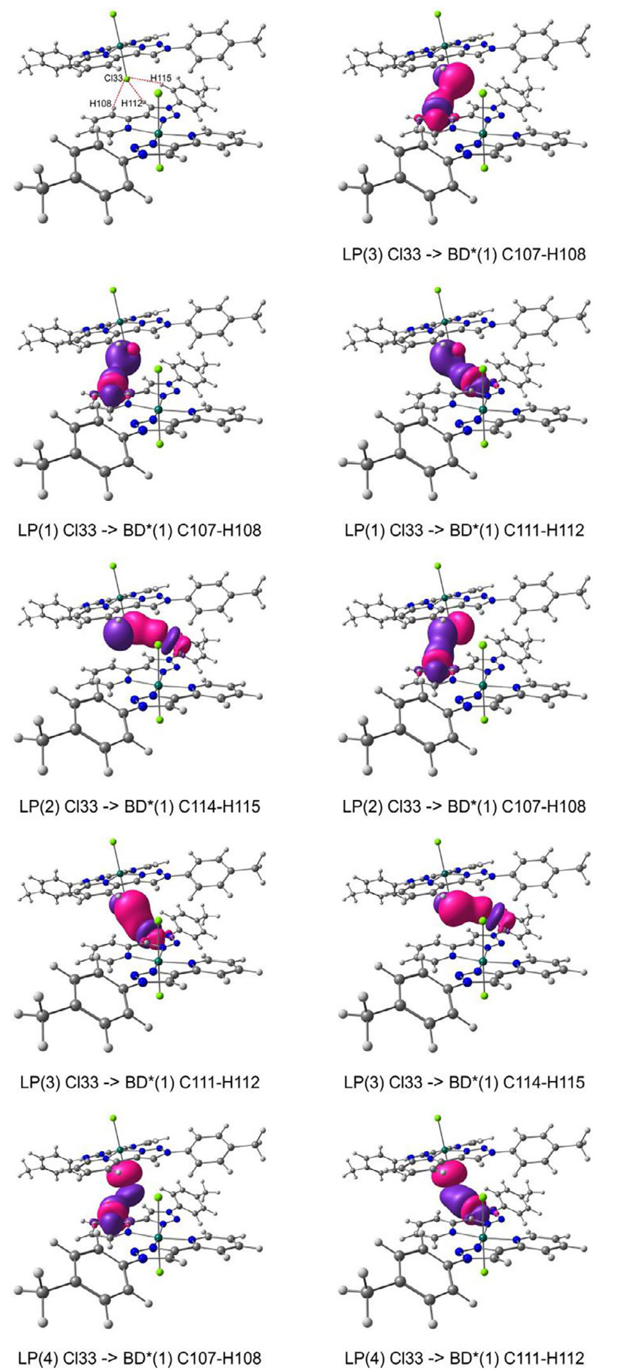

Fig. 10. Selected intermolecular donor–acceptor interactions (between LP on Cl33 and BD* of the indicated CH bonds) involved in intermolecular interactions in the optimized di-molecular model of $[Zn(L^2)_2Cl_2]$. Top left show atom numbers of the atoms involved in the selected interactions. The natural bond orbital (NBO) plots utilise a contour of 0.03 e/Å^3. Colour code of atoms (online version): Zn (turquois), C (grey), N (blue), Cl (green), H (white). (Colour online.)

4. Summary

A first comprehensive series of seven pyridyl-triazole based transition metal coordination compounds, where seven different transition metals, M = Mn (1), Fe (2), Co (3), Ni (4), Cu (5), Zn (6) and Cd (7), coordinated to the same 1,2,3-triazole chromophore, namely 2-(1-(4-methyl-phenyl)-1H-1,2,3-triazol-1-yl)pyridine, has been successfully synthesized and characterized. DFT calcula-

Table 7
Second order perturbation theory interaction energies, $E(2)$, and calculated NBO occupations, for the LP (1-centre nonbonded lone pair) and BD (2-centre bond) NBOs involved in intermolecular interactions in the optimized di-molecular model of $[Zn(L^2)_2Cl_2]$ illustrated in Fig. 10.

Donor		Acceptor	$E(2)$/kJ·mol^{-1}
LP(1) Cl33	→	BD*(1) C107–H108	0.335
LP(1) Cl33	→	BD*(1) C111–H112	2.678
LP(2) Cl33	→	BD*(1) C107–H108	1.799
LP(2) Cl33	→	BD*(1) C114–H115	3.640
LP(3) Cl33	→	BD*(1) C107–H108	0.377
LP(3) Cl33	→	BD*(1) C111–H112	14.853
LP(3) Cl33	→	BD*(1) C114–H115	2.218
LP(4) Cl33	→	BD*(1) C107–H108	0.293
LP(4) Cl33	→	BD*(1) C111–H112	5.188
LP(1) Cl96	→	BD*(1) C13–H14	0.377
LP(1) Cl96	→	BD*(1) C17–H18	2.594
LP(2) Cl96	→	BD*(1) C13–H14	2.092
LP(2) Cl96	→	BD*(1) C20–H21	3.347
LP(3) Cl96	→	BD*(1) C13–H14	0.502
LP(3) Cl96	→	BD*(1) C17–H18	14.602
LP(3) Cl96	→	BD*(1) C20–H21	1.841
LP(4) Cl96	→	BD*(1) C13–H14	0.335
LP(4) Cl96	→	BD*(1) C17–H18	5.104
Donor	**Occupancy/e$^-$**	**Acceptor**	**Occupancy/e$^-$**
LP(1) Cl33	1.995	BD*(1) C107–H108	0.015
LP(2) Cl33	1.991	BD*(1) C111–H112	0.026
LP(3) Cl33	1.976	BD*(1) C114–H115	0.017
LP(4) Cl33	1.922		
LP(1) Cl96	1.995	BD*(1) C13–H14	0.015
LP(2) Cl96	1.991	BD*(1) C17–H18	0.026
LP(3) Cl96	1.976	BD*(1) C20–H21	0.016
LP(4) Cl96	1.921		

tions on the possible spin states of the coordination compounds, are in agreement with the results of the experimentally measured magnetic moment for the paramagnetic coordination compounds (Mn, Fe, Co, Ni and Cu). DFT calculations on the possible isomers of the coordination compounds, showed that the *cis–cis–trans* and the *trans–trans–trans* isomers, with the pyridyl groups *trans* to each other, are the lowest in energy. Single crystal diffraction studies of $[Ni(L^2)_2Cl_2]$ and $[Zn(L^2)_2Cl_2]{\cdot}L^2$, reported in this study, showed them to crystalise as *trans–trans–trans* isomers. The experimentally observed inter-molecular hydrogen bonds, X—H···Cl, in the solid state X-ray structure of $[Zn(L^2)_2Cl_2]$ can from a computational chemistry point of view be described by a donor–acceptor interaction from a filled lone pair NBO on Cl to an empty antibonding NBO on (C—H). The inter-molecular hydrogen bonds can also be described by the QTAIM determined bonding path between Cl and the respective hydrogen.

Acknowledgements

The National Mass Spectroscopy Centre at the University of Wales, Swansea is thanked for supplying the mass spectrometry data. XRD data and structures were supplied by the National Crystallograhy Service at the University of Southampton. KT expresses his gratitude to the Iraqi Government for financial support to conduct the research reported in the UK. This work has received support from the South African National Research Foundation and the Central Research Fund of the University of the Free State, Bloemfontein, South Africa. The High Performance Computing facility of the University of the Free State and the Centre for High Performance Computing CHPC of South Africa are gratefully acknowledged for computer time.

References

[1] R. Huisgen, Centenary Lecture - 1,3-Dipolar Cycloadditions, Proc. Chem. Soc. of London (1961) 357–396, https://doi.org/10.1039/PS9610000357.
[2] C.W. Tornøe, C. Christensen, M. Meldal, Peptidotriazoles on solid phase: [1,2,3]-triazoles by regiospecific copper(I)-catalyzed 1,3-dipolar cycloadditions of terminal alkynes to azides, J. Org. Chem. 67 (2002) 3057–3064, PMID 11975567 2002 10.1021/jo011148j.
[3] V.V. Rostovtsev, L.G. Green, V.V. Fokin, K.B. Sharpless, A stepwise Huisgen cycloaddition process: copper(I)-catalyzed regioselective ligation of azides and terminal alkynes, Angew. Chem., Int. Ed. 41 (2002) 2596–2599, PMID 12203546. DOI:10.1002/1521-3773(20020715)41:14<2596::AID-ANIE2596>3.0.CO;2-4.
[4] D. Schweinfurth, C.Y. Su, S.C. Wei, P. Braunsteind, B. Sarkar, Nickel complexes with "click"-derived pyridyl-triazole ligands: weak intermolecular interactions and catalytic ethylene oligomerisation, Dalton Trans. 41 (2012) 12984–12990, https://doi.org/10.1039/C2DT31805A.
[5] K.M. Tawfiq, G.J. Miller, M.J. Al-Jeboori, P.S. Fennell, S.J. Coles, G.J. Tizzard, C. Wilson, J.H. Potgieter, Comparison of the structural motifs and packing arrangements of six novel derivatives and one polymorph of 2-(1-phenyl-1*H*-1,2,3-triazol-4-yl)pyridine, Acta Cryst. B 70 (2014) 379–389, https://doi.org/10.1107/S2052520614001152.
[6] J. Conradie, M.M. Conradie, K.M. Tawfiq, M.J. Al-Jeboori, S.J. Coles, J.H. Potgieter, Synthesis, characterisation, experimental and electronic structure of novel dichloro(bis{2-[1-(4-methoxyphenyl)-1H-1,2,3-triazol-4-yl-kN3]pyridine-kN})metal(II) compounds, metal = Mn, Co and Ni, J. Mol. Struct. 1161C (2018) 89–99, https://doi.org/10.1016/j.molstruc.2018.02.036.
[7] D. Kumar, V.B. Reddy, An efficient, one-pot, regioselective synthesis of 1,4-diaryl-1*H*-1,2,3-triazoles using click chemistry, Synthesis 10 (2010) 1687–1691, https://doi.org/10.1055/s-0029-1218765.
[8] G.A. Bain, J.F. Berry, Diamagnetic corrections and Pascal's constants, J. Chem. Educ. 85 (2008) 532–536, https://doi.org/10.1021/ed085p532.
[9] Rigaku Corporation, CrystalClear-SM Expert 2.0 r13 Software for Diffractometer, 2011.
[10] O.V. Dolomanov, L.J. Bourhis, R.J. Gildea, J.A.K. Howard, H. Puschmann, OLEX2: a complete structure solution, refinement and analysis program, J. Appl. Cryst. 42 (2009) 339–341, https://doi.org/10.1107/S0021889808042726.
[11] G.M. Sheldrick, A short history of SHELX, Acta Cryst. Sect. A 64 (2008) 112–122, https://doi.org/10.1107/S0108767307043930.
[12] M.J. Frisch, G.W. Trucks, H.B. Schlegel, G.E. Scuseria, M.A. Robb, J.R. Cheeseman, G. Scalmani, V. Barone, B. Mennucci, G.A. Petersson, H. Nakatsuji, M. Caricato, X. Li, H.P. Hratchian, A.F. Izmaylov, J. Bloino, G. Zheng, J.L. Sonnenberg, M. Hada, M. Ehara, K. Toyota, R. Fukuda, J. Hasegawa, M. Ishida, T. Nakajima, Y. Honda, O. Kitao, H. Nakai, T. Vreven, J.A. Montgomery Jr., J.E. Peralta, F. Ogliaro, M. Bearpark, J.J. Heyd, E. Brothers, K.N. Kudin, V.N. Staroverov, R. Kobayashi, J. Normand, K. Raghavachari, A. Rendell, J.C. Burant, S.S. Iyengar, J. Tomasi, M. Cossi, N. Rega, J.M. Millam, M. Klene, J.E. Knox, J.B. Cross, V. Bakken, C. Adamo, J. Jaramillo, R. Gomperts, R.E. Stratmann, O. Yazyev, A.J. Austin, R. Cammi, C. Pomelli, J.W. Ochterski, R.L. Martin, K. Morokuma, V.G. Zakrzewski, G.A. Voth, P. Salvador, J.J. Dannenberg, S. Dapprich, A.D. Daniels, Ö. Farkas, J.B. Foresman, J.V. Ortiz, J. Cioslowski, D.J. Fox, Gaussian 09, Revision D.01, Gaussian, Inc., Wallingford, CT, 2009.
[13] F. Weigend, R. Ahlrichs, Balanced basis sets of split valence, triple zeta valence and quadruple zeta valence quality for H to Rn: design and assessment of accuracy, Phys. Chem. Chem. Phys. 7 (2005) 3297–3305, https://doi.org/10.1039/B508541A.
[14] http://www.chemcraftprog.com/.
[15] E.D. Glendening, J.K. Badenhoop, A.E. Reed, J.E. Carpenter, J.A. Bohmann, C.M. Morales, F. Weinhold, NBO 3.1, Theoretical Chemistry Institute, University of Wisconsin, Madison, WI, USA, 2001.
[16] R.F.W. Bader, A quantum theory of molecular structure and its applications, Chem. Rev. 91 (1991) 893–928, https://doi.org/10.1021/cr00005a013.
[17] F. Cortés-Guzmán, R.F.W. Bader, Complementarity of QTAIM and MO theory in the study of bonding in donor–acceptor complexes, Coord. Chem. Rev. 249 (2005) 633–662, https://doi.org/10.1016/j.ccr.2004.08.022.
[18] J.I. Rodríguez, R.F.W. Bader, P.W. Ayers, C. Michel, A.W. Götz, C. Bo, A high performance grid-based algorithm for computing QTAIM properties, Chem. Phys. Lett. 472 (2009) 149–152, https://doi.org/10.1016/j.cplett.2009.02.081.
[19] G. te Velde, F.M. Bickelhaupt, S.J.A. van Gisbergen, C.F. Guerra, E.J. Baerends, J. G. Snijders, T. Ziegler, Chemistry with ADF, J. Comp. Chem. 22 (2001) 931–967, https://doi.org/10.1002/jcc.1056.
[20] C. Fonseca Guerra, J.G. Snijders, G. te Velde, E.J. Baerends, Towards an order-N DFT method, Theor. Chem. Acc. 99 (1998) 391–403, https://doi.org/10.1007/s002140050353.
[21] ADF2013, SCM, Theoretical Chemistry, Vrije Universiteit, Amsterdam, The Netherlands, 2013. http://www.scm.com.
[22] L. Jiang, Z. Wang, S.-Q. Bai, T.S. Andy, Hor, "Click-and-click" – hybridised 1,2,3-triazoles supported Cu(I) coordination polymers for azide–alkyne cycloaddition, Dalton Trans. 42 (2013) 9437–9443, https://doi.org/10.1039/C3DT50987G.
[23] S.K. Vellas, J.E.M. Lewis, M. Shankar, A. Sagatova, J.D.A. Tyndall, B.C. Monk, Ch. M. Fitchett, L.R. Hanton, J.D. Crowley, $[Fe_2L_3]^{4+}$ cylinders derived from bis (bidentate) 2-pyridyl-1,2,3-triazole "Click" ligands: synthesis, Struct. Explor. Biol. Act., Mol. 18 (2013) 6383–6407, https://doi.org/10.3390/molecules18066383.
[24] W.J. Geary, The use of conductivity measurements in organic solvents for the characterisation of coordination compounds, Coord. Chem. Rev. 7 (1971) 81–122, https://doi.org/10.1016/S0010-8545(00)80009-0.
[25] D. Czakis-Sulikowska, A. Czylkowska, Complexes of Mn(II), Co(II), Ni(II) and Cu (II) with 4,4'-bipyridine and dichloroacetates, J. Therm. Anal. Cal. 71 (2003) 395–405, https://doi.org/10.1023/A:1022879120867.

[26] D. Czakis-Sulikowska, A. Czylkowska, Synthesis, thermal and other studies of 2,4'-bipyridine-dichloroacetato complexes of Mn(II), Co(II), Ni(II) and Cu(II), J. Therm. Anal. Cal. 76 (2004) 543–555, https://doi.org/10.1023/B:JTAN.0000028033.91256.c6.
[27] T. Steiner, The hydrogen bond in the solid state, Angew. Chem., Int. Ed. 41 (2002) 48–76, https://doi.org/10.1002/1521-3773(20020104)41:1<48::AID-ANIE48>3.0.CO;2-U.
[28] G.A. Jeffrey, An Introduction to Hydrogen Bonding, Oxford University Press, New York and Oxford, 1997.
[29] Cambridge Structural Database (CSD), Version 5.38, May 2017 update, Cambridge, UK, 2017 C.R. Groom, F.H. Allen Angew. Chem. Int. Ed. 53 (2014) 662–671.
[30] R.F.W. Bader, A bond path: a universal indicator of bonded interactions, J. Phys. Chem. A 102 (1998) 7314–7323, https://doi.org/10.1021/jp981794v.
[31] O. Mó, M. Yáñez, J. Elguero, Cooperative (nonpairwise) effects in water trimers: an ab initio molecular orbital study, J. Chem. Phys. 97 (1992) 6628–6638, https://doi.org/10.1063/1.463666.
[32] E. Espinosa, E. Molins, C. Lecomte, Hydrogen bond strengths revealed by topological analyses of experimentally observed electron densities, Chem. Phys. Lett. 285 (1998) 170–173, https://doi.org/10.1016/S0009-2614(98)00036-0.
[33] E. Espinosa, E. Molins, Retrieving interaction potentials from the topology of the electron density distribution: the case of hydrogen bonds, J. Chem. Phys. 113 (2000) 5686–5694, https://doi.org/10.1063/1.1290612.
[34] U. Koch, P.L.A. Popelier, Characterization of C-H-O hydrogen bonds on the basis of the charge density, J. Phys. Chem. 99 (1995) 9747–9754, https://doi.org/10.1021/j100024a016.
[35] P.L.A. Popelier, Characterization of a dihydrogen bond on the basis of the electron density, J. Phys. Chem. A 102 (1998) 1873–1878, https://doi.org/10.1021/jp9805048.